Pergamon

Acta Materialia 50 (2002) 13–21

Acta MATERIALIA

www.elsevier.com/locate/actamat

Coarsening dynamics of self-accommodating coherent patterns

Y.H. Wen [a, b,*], Y. Wang [b], L.Q. Chen [a]

[a] *Department of Materials Science and Engineering, The Pennsylvania State University, University Park, PA 16802, USA*
[b] *Department of Materials Science and Engineering, The Ohio State University, Columbus, OH 43210, USA*

Received 18 December 2000; received in revised form 3 September 2001; accepted 6 September 2001

Abstract

The coarsening kinetics of self-accommodating coherent domain structures is investigated using computer simulations based on a continuum phase-field model. The domain structures are produced from coherent hexagonal to orthorhombic phase transformations. It is found that the long-range elastic interactions arising from the lattice accommodation among different orientation domains of the orthorhombic phase dominate the domain morphologies and the kinetics of domain coarsening. It is shown that the long-range elastic interactions result in several new features for the domain coarsening as compared to normal grain growth. For example, the domain growth rate is reduced significantly and the growth exponent becomes a function of the relative contribution of the elastic energy reduction to the total driving force. In general, the elastic interaction is in favor of fine domains. Although triple junctions are dominant in the microstructure, a significant amount of quadrojunctions exist throughout the domain coarsening process. The average number of sides of the domain is also reduced.

Keywords: Computer simulation; Coarsening kinetics; Phase transformation

1. Introduction

Grain growth and domain growth driven by the reduction in the total interfacial energy have been extensively studied for decades. It is generally agreed that for this type of growth process, there exists a scaling regime in which the domain or grain size distribution is independent of time, whereas the average domain or grain size increases following a simple power growth law in the absence of pinning force at the boundaries such as small particles and/or pores as well as by solute segregation etc [1]:

$$R^2 - R_0^2 = Kt, \tag{1}$$

where R is the average grain size at time t, R_0 is the initial grain size, and K is the kinetic constant which is generally a function of temperature.

Many of the experimental isothermal grain growth data correspond to empirical equations of the form

$$R = kt^n, \tag{2}$$

* Corresponding author. Fax: +1-614-292-1537.
E-mail address: ywen@ues.com (Y.H. Wen).

1359-6454/02/$22.00
PII: S1359-6454(01)00335-4

assuming that $R_0 \ll R$. The exponent n found experimentally is, in most cases, smaller than the theoretically predicted value of 1/2 indicting the existence of some kinds of pinning force in real materials (see e.g. [2] for some recent results).

There is a class of domain structures in which the domain morphologies are strongly influenced by the long-range elastic interactions arising from the accommodation of lattice misfit among domains. For this type of domain structures, domain coarsening is driven by the reduction in the total interfacial energy as well as the elastic strain energy. A critical question is whether or not the conventional grain growth theories, which developed under the assumption that interfacial energy is the sole driving force, can be applied to predict or describe the domain coarsening process in the presence of long-range elastic interactions. To answer this question, we consider a particular example of domain structures produced from hexagonal to orthorhombic transformations. Recently, we showed that the long-range elastic interactions dominate the domain morphologies in these systems [3–5]. The main purpose of this work is to examine the effect of elastic interactions on the kinetics of domain coarsening and examine the applicability of conventional grain growth theories.

2. The computer model

Detailed descriptions of the model can be found in our previous work [3,4]. Here we just give a brief introduction. The hexagonal→orthorhombic transformation produces three pairs of orientation domains [5]. Three order parameter fields, $(\eta_1(\mathbf{r}, t), \eta_2(\mathbf{r}, t), \eta_3(\mathbf{r}, t))$, where $\mathbf{r}$ and t are the spatial coordinate vector and time, respectively, are required to characterize the development of the multi-domain structures, including the evolution of shape, size, and spatial arrangement of the three pairs of orientation domains. The temporal evolution of the order parameter field then completely describes the domain structure evolution, which can be obtained by solving the time-dependent Ginzburg–Landau (TDGL) equations,

$$\frac{\partial \eta_p(\mathbf{r}, t)}{\partial t} = -L\frac{\delta F}{\delta \eta_p(\mathbf{r}, t)} + \xi_p(\mathbf{r}, t); \; p = 1, 2, 3 \tag{3}$$

where L is the kinetic coefficient that determines the domain-wall mobility, F is the total free energy of the system which includes the chemical free energy and elastic energy, and $\xi_p(\mathbf{r}, t)$ is the Langevin noise term which is taken to be Gaussian distributed and its correlation properties meet the requirements of the fluctuation-dissipation theorem [6].

The chemical free energy as a functional of the order parameter field is modeled by a diffuse-interface description, i.e.

$$F_{\text{chem}} = \int_V \left[\frac{1}{2}\sum_{p=1}^{3} \lambda(\nabla \eta_p)^2 + f(\eta_1, \eta_2, \eta_3)\right] \mathrm{d}V \tag{4}$$

where the integration is carried out over the entire system volume V. The gradient terms in Eq. (4) provide an energy penalty to inhomogeneity in the order-parameter field which takes place at domain boundaries and λ is the gradient energy coefficient.

The local specific free energy $f(\eta_1, \eta_2, \eta_3)$ in Eq. (4) defines the basic bulk thermodynamic properties of the system. As argued in [3], a simple functional of the form

$$f(\eta_1, \eta_2, \eta_3) = \frac{1}{2}A_1(\eta_1^2 + \eta_2^2 + \eta_3^2) - \frac{1}{4}A_2(\eta_1^4 + \eta_2^4 + \eta_3^4) + \frac{1}{6}A_3(\eta_1^2 + \eta_2^2 + \eta_3^2)^3 \tag{5}$$

provides a qualitatively correct thermodynamic description of the system, where A_1, A_2 and A_3 are phenomenological constants.

The elastic strain energy of an arbitrary coherent multi-domain structure can be calculated using the linear elasticity theory of Khachaturyan [7]. Assuming that the local stress-free transformation strain can be described through the order parameter field as

$$\epsilon_{ij}^{0}(\mathbf{r}) = \sum_{p=1}^{3} \epsilon_{ij}^{0}(p)\eta_p^2(\mathbf{r}), \tag{6}$$

where $\epsilon_{ij}^{0}(p)$ is the stress-free transformation strain

of pair p, then the elastic strain energy for an elastically homogeneous system can be written in the following close form (see [3] and references therein),

$$E_{el} = \frac{V}{2}C_{ijkl}\bar{\epsilon}_{ij}\bar{\epsilon}_{kl} - VC_{ijkl}\bar{\epsilon}_{ij}\sum_{p=1}^{3}\epsilon^{o}_{kl}(p)\overline{\eta_p^2(\mathbf{r})} + \frac{V}{2}C_{ijkl}\sum_{p=1}^{3}\sum_{q=1}^{3}\epsilon^{o}_{ij}(p)\epsilon^{o}_{kl}(q)\overline{\eta_p^2(\mathbf{r})\eta_q^2(\mathbf{r})} - \frac{1}{2}\sum_{p=1}^{3}\sum_{q=1}^{3}{\int}'\frac{d^3\mathbf{g}}{(2\pi)^3}B_{pq}(\mathbf{n})\{\eta_p^2(\mathbf{r})\}^{*}_{\mathbf{g}}\{\eta_q^2(\mathbf{r})\}_{\mathbf{g}} \quad (7)$$

where $\overline{(\ldots)}$ represents the volume average of $(\ldots)$, C_{ijkl} is the elastic constant of the parent phase, $\bar{\epsilon}_{ij}$ is the homogeneous strain, $\mathbf{g}$ is the spatial coordinate vector in the reciprocal space, $\int'$ means the point $\mathbf{g} = 0$ is excluded in the integration, $\{\eta_p^2(\mathbf{r})\}_{\mathbf{g}}$ is the Fourier transform of $\eta_p^2(\mathbf{r})$, $\{\eta_p^2(\mathbf{r})\}^{*}_{\mathbf{g}}$ is the complex conjugate of $\{\eta_p^2(\mathbf{r})\}_{\mathbf{g}}$, and

$$B_{pq}(\mathbf{n}) = n_i\sigma^{o}_{ij}(p)\Omega_{jk}(\mathbf{n})\sigma^{o}_{kl}(q)n_l \quad (8)$$

where $\mathbf{n} = \mathbf{g}/g$ is a unit vector in reciprocal space and n_i is its ith component, $\sigma^{o}_{ij}(p) = C_{ijkl}\epsilon^{o}_{kl}(p)$ and $\Omega_{ij}(\mathbf{n})$ is a Green function tensor which is inverse to the tensor $\Omega^{-1}_{ij}(\mathbf{n}) = C_{iklj}n_kn_l$. Please note that all the information with regard to the elastic properties, the stress-free transformation strain, and the transformation crystallography are contained in the function $B_{pq}(\mathbf{n})$ whereas the mesoscale domain morphology is described by $\{\eta_p^2(\mathbf{r})\}_{\mathbf{g}}$. The macroscopic shape change of the crystal due to the transformation is given by the homogeneous strain, $\bar{\epsilon}_{ij}$.

The hexagonal to orthorhombic transformation can be described as a distortion of the hexagonal basal plane along any of the three equivalent $\langle 11\bar{2}0\rangle_{\text{h.c.p.}}$ directions, leaving the c parameter essentially unchanged [8]. As a result, the domain evolution during the hexagonal to orthorhombic transformation can be effectively modeled in two dimensions (on the basal plane) without losing any essential physics. The corresponding stress-free transformation strain tensors of the three pairs of orientation domains can be described by [3,4]

$$\epsilon^{o}(1) = \epsilon_s\begin{pmatrix}1 & 0\\ 0 & -1\end{pmatrix},\quad \epsilon^{o}(2) = \epsilon_s\begin{pmatrix}-1/2 & \sqrt{3}/2\\ \sqrt{3}/2 & 1/2\end{pmatrix},\quad \epsilon^{o}(3) = \epsilon_s\begin{pmatrix}-1/2 & -\sqrt{3}/2\\ -\sqrt{3}/2 & 1/2\end{pmatrix}, \quad (9)$$

where ϵ_s represents the magnitude of the shear deformation.

The dimensionless form of the kinetic Eq. (3) is achieved by introducing a reduced time, defined as $\tau = L|\Delta f|t$, and reduced spatial coordinates, defined as $u_i = x_i/l$. In these definitions, Δf is the depth of the potential well defined as $\Delta f = |\min f(\eta_1, \eta_2, \eta_3)| = |f(\eta_0, 0, 0)|$ and l is the length scale assigned to the computational grid size. Substituting these reduced variables into Eq. (3) and using Eqs. (5) and (7) for defining the free energy functional, we get the dimensionless form of the kinetic equation:

$$\frac{\partial\eta_p(\mathbf{u},\tau)}{\partial\tau} = -\{-\beta\nabla^2(\eta_p(\mathbf{u},\tau)) + \frac{\partial f_a}{\partial\eta_p(\mathbf{u},\tau)} + \alpha\frac{\delta E'_{el}}{\delta\eta_p(\mathbf{u},\tau)}\} + \xi'_p(\mathbf{u},\tau) \quad (10)$$

where

$$\alpha = \frac{4G\epsilon_s^2}{|\Delta f|},\ \beta = \frac{\lambda}{l^2|\Delta f|},\quad f_a = \frac{1}{2}a_1(\eta_1^2+\eta_2^2+\eta_3^2) - \frac{1}{4}a_2(\eta_1^4+n_2^4+\eta_3^4) + \frac{1}{6}a_3(\eta_1^2+\eta_2^2+\eta_3^2)^3 \quad (11)$$

with

$$a_1 = \frac{A_1}{|\Delta f|},\ a_2 = \frac{A_2}{|\Delta f|},\ a_3 = \frac{A_3}{|\Delta f|},$$

and

$$\frac{\delta E'_{el}}{\delta\eta_p(\mathbf{u},\tau)} = \frac{2\eta_p(\mathbf{u},\tau)}{4G\epsilon_s^2}[-C_{ijkl}\epsilon^{a}_{ij}\epsilon^{o}_{kl}(p)$$

$$+\sum_{q=1}^{3}[C_{ijkl}\epsilon_{ij}^{0}(p)\epsilon_{kl}^{0}(q)\eta_q^2(\mathbf{u},\tau) - \{B_{pq}(\mathbf{n})\{\eta_q^2(\mathbf{u},\tau)\}_{\mathbf{g}'}\}_{\mathbf{u}}]]$$

where

$$\mathbf{g}' = \mathbf{g}l,$$

$$\langle \xi'_p(\mathbf{u},\tau)\xi_p(\mathbf{u}',\tau')\rangle = \frac{2k_BT}{|\Delta f|l^3}\delta(\mathbf{u}-\mathbf{u}')\delta(\tau-\tau')$$

To solve Eq. (10), two dimensionless parameters, namely α and β as defined in Eq. (11), need to be specified. These two parameters characterize the relative contributions of the specific strain energy and gradient energy with respect to the chemical driving force. By setting α and β equal to 15 and 0.1, respectively, all the essential features of domain structure patterns observed by experiments have been well reproduced by our computer simulations [3,4]. In this work, we will keep β unaltered and vary α between 0 and 15 (thus changes the ratio of α/β) to study the influence of the strength of long-range elastic interactions on the coarsening kinetics, where the case with $\alpha = 0$ corresponds to the conventional antiphase domain coarsening or grain growth without the elastic interaction. The simulations are carried out on a finer mesh with 1536×1536 grid points for the sake of accuracy of the calculations. All other input data including the initial condition, noise-term related parameters, the spatial grid size, and the time step of the integration etc. are exactly the same as those employed in [3].

3. Simulation results and discussion

3.1. Domain structure

Since our focus is on the domain coarsening process, domain structures and coarsening behavior are characterized after the entire system has transformed into the orthorhombic phase ($\tau \geq 50$). Fig. 1 shows the multi-domain structure of the orthorhombic phase in several cases with different values of α. In the simulated micrographs, bright, grey and black areas represent three pairs of orientation domains, respectively [4]. We have chosen to show only the results at the final stage of the simulation ($\tau = 2000$).

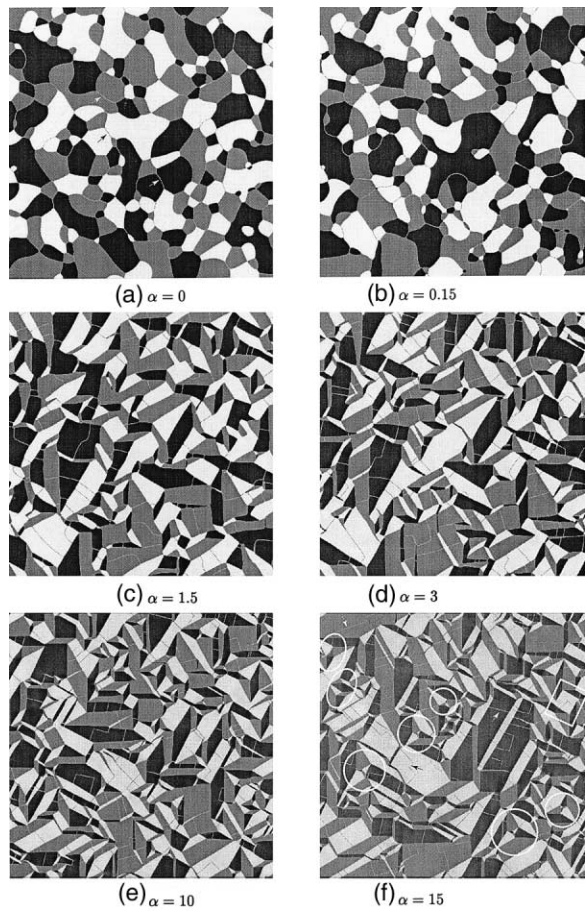

Fig. 1. Influence of elastic energy with various strength on the microstructure at the final stage of the simulation ($\tau = 2000$).

From Fig. 1, it is evident that the elastic interactions have a strong influence on the domain morphologies. In the case without any elastic interaction [Fig. 1(a)] or with very weak elastic interaction [Fig. 1(b)], the domains have isotropic shapes with the domain boundaries meeting at primarily triple junctions. The angles between the domain walls meeting at the triple junctions are about 120°, which is consistent with the isotropic interfacial energy assumed in the simulation. In contrast, when the elastic interactions become stronger, the domains become highly anisotropic in

shape [Fig. 1(c)–(f)]. The domain structures are very similar over a wide range of values of α indicating that these cases are dominated by elastic interactions. For example, junction angles are multiples of 30°, such as 30, 60, 90, 120, and 150°. A close examination of the crystallographic relationship among the orientation domains revealed that essentially all the domain boundaries produced from our computer simulations are twin planes $\{1\ 1\ 0\}_O$, or $\{1\ 3\ 0\}_O$ [5,8]. The intersection of these planes form a number of complex domain patterns [refer to those areas enclosed by circles or ellipses in Fig. 1(f)] which agree very well with experimental observations [8–11].

3.2. Domain growth rate

Irrespective of the strength of the elastic interactions the overall domain size increases with time. However, the rate of domain coarsening depends strongly on the strength of the elastic interactions. To compare the domain coarsening rates for the cases presented in Fig. 1, we calculated the number of domains and their area by counting the number of grid points within each domain. It should be pointed out that the domain area S is a more valid representation of domain size as opposed to the radius R. However, the latter was used in earlier works for simplicity. To compare with those results, the domain size R was approximated by $R = \sqrt{S}$. The average domain size, namely $<R>$, at a given time is obtained by averaging over all the domains in the system. In Fig. 2, we plot the average domain size as a function of time for those cases. As can be seen the coarsening process slows down dramatically with increasing elastic contributions, which is obvious by comparing the $<R>$ at any given time (τ). If we fit the data to the equation $R^n - R_0^n = Kt$ using a multi-parameter nonlinear least-square fit to extract the growth exponent n and constant K, we find that the exponent n, unlike the constant K, increases monotonically with increasing elastic contribution. For the case with $\alpha = 0$, it is about 2.0, in agreement with the theoretical prediction given in Eq. (1) and previous works on antiphase domain coarsening [12,13] as well as on grain growth in pure systems [14,15]. However, for the case with $\alpha = 15$, the exponent

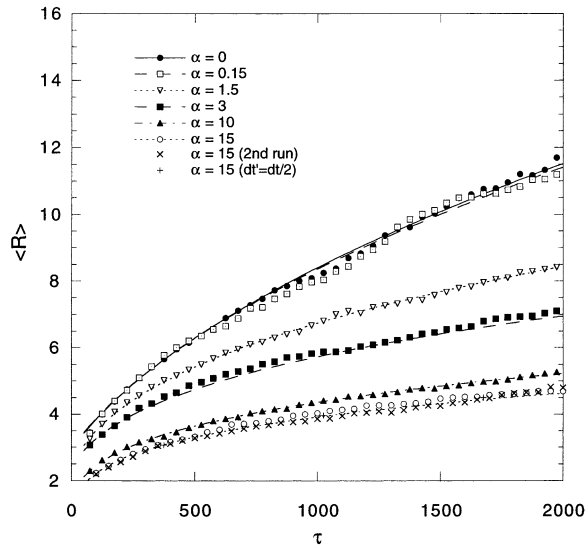

Fig. 2. Mean radius of domains vs. time under various strengths of elastic interactions. Data are fitted into equations $R^n - R_0^n = Kt$ and the fitted curves are shown together with the discrete numerical results.

n is approximately 4.1. These results indicate that the elastic interactions slow down the coarsening process by mainly increasing the growth exponent n. We note that there is no unique value for n, instead it depends on the relative strength of elastic interactions.

One may have noticed that the $<R>$ at $\tau = 50$ decreases monotonically with increasing α, although all the simulations are started from exactly the same initial condition. This is in line with the analysis of domain number at $\tau = 50$ which increases with increasing α. This may be attributed to the strain-induced autocatalytic effect of nucleation.

To exclude any possible artifact, we studied the dependence of the simulation results for two extreme cases, namely α=0 and α=15, on some numerical input data. First, the time increment $\Delta\tau$ for the numerical integration of the kinetic equations was examined. The result is shown in Fig. 2 (+) for the case with $\alpha = 15$ where the $\Delta\tau$ is reduced to 0.05. The results are almost identical to the original data with $\Delta\tau = 0.1$ (○), indicating that the selected time step is appropriate and any further decrease in $\Delta\tau$ has no significant effect on the

simulation results. We also found that the simulation results are independent of the strength of the noise term and the initial configuration (×), which was realized by using different seed numbers for the random number generator introduced at the nucleation stage and different strengths. The possible effect of grid size on the simulation results was also investigated. The results with meshes 1024×1024 and 2048×2048 are shown in Fig. 3 together with the original results for the two cases with $\alpha = 15$ and $\alpha = 0$. The grid size, namely du_x and du_y, for the two testing meshes are adjusted accordingly to ensure that their system size is the same as that of the original mesh. The calculations with mesh 2048×2048 are terminated at an earlier stage ($\tau = 1000$) because of their high demand for memory and cpu time. All the simulation results are almost identical in terms of the characteristic morphology and kinetics, irrespective of the grid size.

From the microstructures shown in Fig. 1, one can find the existence of antiphase domain boundaries [e.g., see arrows in Fig. 1(a) and (f)]. In order to clarify if the above obtained coarsening kinetics is influenced by the presence of these antiphase domain boundaries, we have repeated calculations

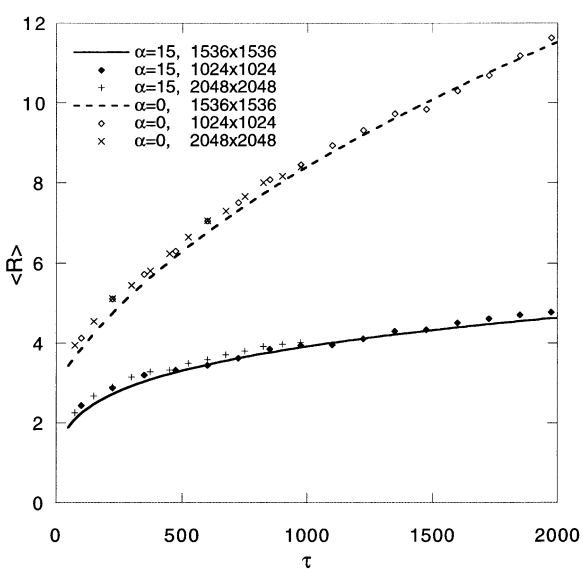

Fig. 3. Influence of grid size on the coarsening kinetics of domain structure.

for the two cases with $\alpha = 15$ and $\alpha = 0$ by removing antiphase domain boundaries at the nucleation stages. Our results show that the removing of these antiphase domain boundaries has no significant influence on the growth exponent n while the parameter K is higher for both cases.

Qualitatively, the slow-down in coarsening kinetics by elastic interaction can be explained by the formation of some collective multi-domain morphological patterns as a result of the interplay between the elastic energy and the interfacial energy. Those patterns highlighted in Fig. 1(f) generally involve three different orientation domains with roughly equal volume (or area) fractions. Within such patterns, the average stress-free transformation strain ($\bar{\epsilon}$) is given by

$$\bar{\epsilon} = \frac{1}{3}\epsilon^{o}(1) + \frac{1}{3}\epsilon^{o}(2) + \frac{1}{3}\epsilon^{o}(3)$$
$$= \frac{1}{3}\epsilon_s\begin{pmatrix}1 & 0\\ 0 & -1\end{pmatrix} + \frac{1}{3}\epsilon_s\begin{pmatrix}-1/2 & \sqrt{3}/2\\ \sqrt{3}/2 & 1/2\end{pmatrix} + \frac{1}{3}\epsilon_s\begin{pmatrix}-1/2 & -\sqrt{3}/2\\ -\sqrt{3}/2 & 1/2\end{pmatrix} = 0. \quad (12)$$

It can be seen that the average stress-free transformation strain can be completely canceled out within such a pattern. However, this treatment is reasonable only near the central region of the pattern where three variants meet together. Inside each particular variant of the domain structure, the stress-free transformation strain still presents. When the overall pattern is relatively small the elastic energy associated with them may be negligible. However, when this pattern grows driven by the interfacial energy reduction the elastic energy may be significant. Therefore, small collective patterns are favorable for reducing elastic energy. So there is an interplay between elastic energy and interfacial energy. When the elastic interaction is dominant, one may expect some fine self-accommodating domain structures. That is exactly the case as observed in our simulation. For example, one can find some very small domains especially in central regions of some star patterns even at the final stage of the simulation [enclosed by white circles in Fig. 1(f)].

3.3. Domain size and topological distributions

Normal grain growth is characterized by a quasi-stationary distribution of grain sizes in the scaling stage. The grain size distribution is relatively narrow, with the maximum grain size being of the order of 2.5–3 times the arithmetic mean grain size. In Fig. 4 we show the domain size distributions for both cases with $\alpha = 0$ and $\alpha = 15$. In the plot, x-axis stands for $\log(R/\langle R\rangle)$, and y-axis represents the normalized frequency of occurrence (with respect to its maximum value). As can be seen, the distribution with the elastic interaction (squares) is broader and this effect is more significant at the negative branch of the x-axis which means that the main contribution is from the existence of some very small domains in the case with strong elastic interaction. Taking two curves at $\tau = 2000$ as an example, if we count domains with 10%+ frequency, then the R is approximately in the range of 0.03~3.8 $\langle R\rangle$ and 0.14~2.4 $\langle R\rangle$ for the cases with and without elastic strain energy contribution ($\alpha = 15$ and $\alpha = 0$, respectively). While the size distribution in the case without elastic interactions is in line with observations of normal grain growth, it is much broader when the long-range elastic interactions are present. For example, there is a significant amount of domains of sizes as small as 3% of the mean value. This can be verified by comparing those small domains in the central region of those patterns enclosed by white circles with some big blocks elsewhere in Fig. 1(f).

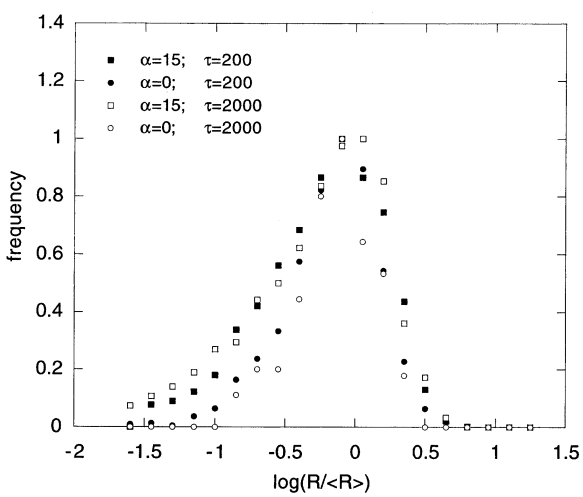

Fig. 4. Influence of elastic interactions on the domain size distributions at two different stages of the coarsening process.

There are a number of interesting observations with regard to the topological features of the domain structures. We first analyze how the domains assemble themselves to fill the whole space by counting their neighboring domains (either through corner or edge). In Fig. 5(a), we plot its mean value against evolution time. It can be seen that the mean number of neighbors is very close to six with $\alpha = 15$ or $\alpha = 0$ in all the time span although the value for the case with elastic interaction is slightly smaller. Further statistic information can be found in Fig. 5(b) where we plot the relative frequency of occurrence for a certain number of neighbors for the domain structure at the final stage ($\tau = 2000$). As can be seen, the two curves are very similar and the majority of domains have approximately four to six neighbors for both cases. Based on these results, it is clear that the elastic energy does not significantly affect the number of contacting domains in the domain structure.

It is well known that junctions where grains meet in a two-dimensional grain structures are primarily triple junctions. Our simulation results, as shown in Fig. 6(a), are in line with this observation. For the domain structures without elastic interactions, essentially all junctions are triple junctions. However, for the case with strong elastic interaction, there is a significant amount of quadro-junctions which can be clearly seen in Fig. 6(b). There are about 35 quadrojunctions at the final figure of the simulation ($\tau = 2000$), which is quite stable against coarsening. This kind of junction is related to the formation of the star pattern as illustrated by the insert in Fig. 6(b).

Finally, we analyze the number of sides for a domain. A side is defined as a common line (either curved or straight in two dimensions) between two contacting domains with a length which is larger than a rather arbitrary chosen length, i.e., we do not count those with less than 20 grid points, keeping in mind that the whole system contains 1536×1536 grid points; sides with less than 20 grid points means the length is less than ~1% of the system dimension. This seems to be a reasonable

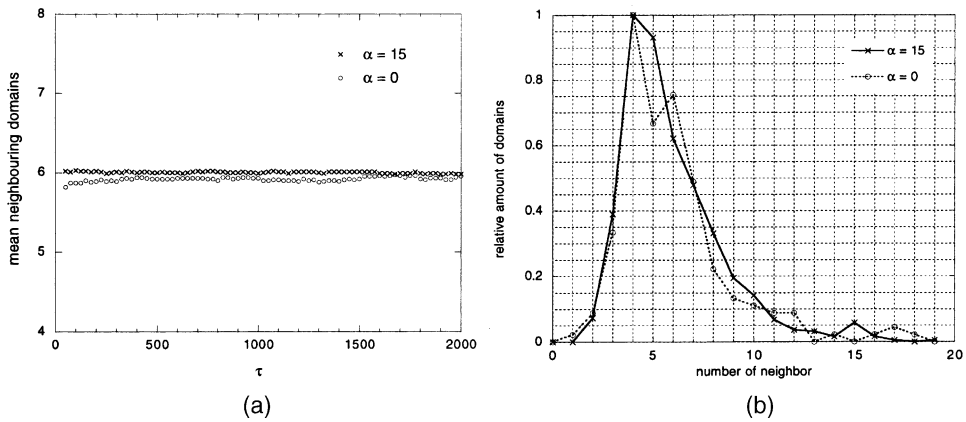

Fig. 5. Influence of elastic interaction on the topological aspect of the domain structure. (a) The average amount of neighbors with time; (b) Neighbors distribution statistics at the final stage (τ=2000).

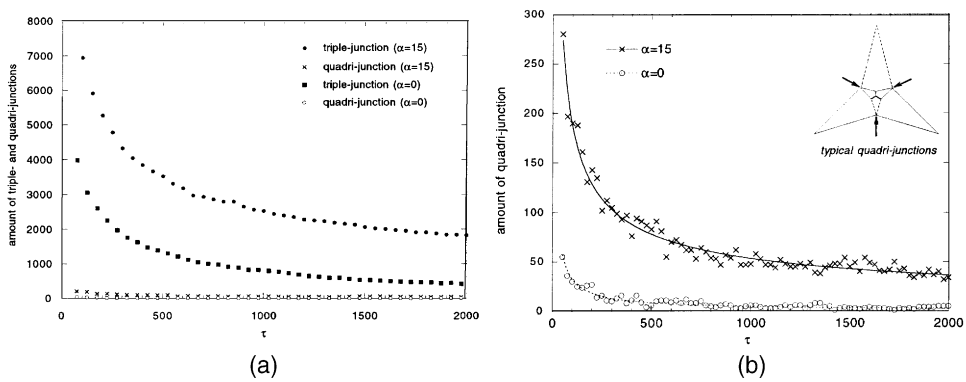

Fig. 6. (a) Amount of triple and quadrojunctions with and without elastic interactions; (b) the amount of quadrojunctions during the coarsening process. Schematic illustration on the top-right corner shows examples of the quadrojunction.

choice. In Fig. 7(a), we show the evolution of the mean number of sides against time based on the above measurement. It is found that the mean sides are roughly time independent during the coarsening process and the elastic interaction reduces approximately one side on average. Side statistics shown in Fig. 7(b) demonstrate that there is a shift leftward for the case with $\alpha = 15$ (solid line) with respect to the case with $\alpha = 0$. Accordingly, the maximum frequency for $\alpha = 0$ takes place at five sides, in agreement with those results obtained from computer simulations of grain growth. In the case with $\alpha = 15$, however, the maximum frequency of occurrence is at four, which may be attributed to the fact that the principal morphology of a single orientation domain is diamond-like and most of the domains have four sides in some well self-accommodated pattern such as the star pattern, as illustrated in the insert of Fig. 6(b).

4. Concluding remarks

The coarsening kinetics of coherent multidomain structures is studied using the continuum phase-field model. It is demonstrated that the long-range elastic interactions among different orientation domains of the orthorhombic phase not only dominate the domain morphologies but also strongly influence the kinetics of domain coarsen-

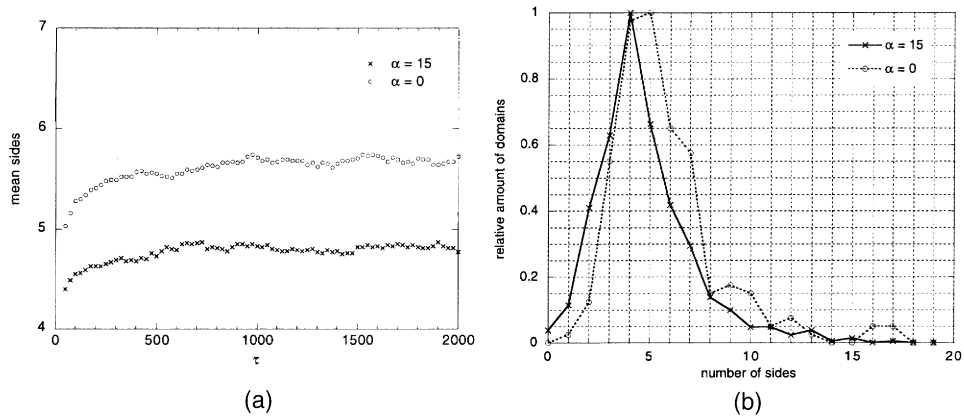

Fig. 7. (a) Influence of elastic interactions on the mean sides of domains during the coarsening process; (b) relative frequency of occurrence for certain number of sides at $\tau = 2000$.

ing. The predicted domain growth exponent during coarsening is dependent on the relative contributions of elastic strain energy and interfacial energy. The average domain size and topological distributions are calculated and compared with those obtained in systems without elastic interactions. It is found that the domain size distribution is significantly broader due to the presence of elastic interactions. This is mainly contributed by the presence of a significant amount of well self-accommodated small domains in the case of elastic interactions. The elastic interaction also has an effect on the topology of the domain structure. In particular, there are a significant number of quadrojunctions present as a result of elastic interactions.

Acknowledgements

The authors are grateful for the financial support from NSF under grant number DMR-96-33719 (Chen) and DMR-9703044 (Wang and Wen). The simulation was performed at the San Diego Supercomputer Center and the Pittsburgh Supercomputing Center.

References

[1] Reed-Hill RE, Abbaschian R. Physical metallurgy principles. 3rd ed. Boston: PWS Publishing Company, 1994.
[2] Gil FJ, Planell JA. Mater Sci Eng A 2000;A283:17.
[3] Wen YH, Wang Y, Chen LQ. Phil Mag A 2000;80:1967.
[4] Wen YH, Wang Y, Chen LQ. Acta mater 1999;47:4375.
[5] Wen YH, Wang Y, Bendersky LA, Chen LQ. Acta mater 2000;48:4125.
[6] Lifshitz EM, Pitaevskii LP. Statistical physics. Oxford: Pergamon Press, 1980.
[7] Khachaturyan AG. Theory of structural transformations in solids. New York: John Wiley & Sons, 1983.
[8] Pierron X, De Graef M, Thompson AW. Phil Mag A 1998;77:1399.
[9] Manolikas C, Amelinckx S. Phys stat sol (a) 1980;60:607.
[10] Kitano Y, Kifune K. Ultramicroscopy 1991;39:279.
[11] Muraleedharan K, Banerjee D. Scripta metall 1993;29:527.
[12] Allen SM, Cahn JW. Acta metall 1979;27:1085.
[13] Allen SM, Cahn JW. Acta metall 1979;27:1017.
[14] Bolling GF, Winegard WC. Acta metall 1958;6:283.
[15] Drolet JP, Galibois A. Acta metall 1968;16:1387.